MASS, HEAT, AND MOISTURE BUDGET ANALYSES OF BOMEX PHASE 4

by

JAAKKO HELMINEN

Department of Meteorology
University of Helsinki

Abstract

A/B-scale mass, heat, and moisture budgets are examined over the tropical Atlantic Ocean during Phase 4 (13, 18–20, 22, and 28 July, 1969) of the Barbados Oceanographic and Meteorological Experiment (BOMEX). Using a compositing technique the available one-day periods with a 3-hour observation interval are classified into a weakly disturbed class 1 (2 days; $N = 16$), which includes weak and decaying cloud clusters, and a strongly disturbed class 2 (4 days; $N = 32$) characterized by organized cloud clusters. In class 1 a divergent layer from $p^\star = 200$ mb to $p^\star = 280$ mb and a convergent one from $p^\star = 380$ mb to $p^\star = 420$ mb were found. There is also a large heat sink between $p^\star = 200$ mb and $p^\star = 480$ mb. In class 2 low-level convergence, upward motion, and a large apparent heat source from $p^\star = 50$ mb upwards were detected. The moisture budget results scatter widely in the vertical in both classes. Some reasons for this partial failure are discussed.

1. Introduction

It is well known that the intertropical convergence zone (ITCZ) with strong cumulus convection is one characteristic feature of the tropical oceanic atmosphere. Furthermore, the cumuli within the ITCZ are typically organized cloud clusters (Joint Organizing Committee Study Group, [5]), which still pose a challenging problem to the cumulus parameterization theories (ARAKAWA and SCHUBERT [1] and BETTS [2]).

In assessing the cumulus ensemble properties of the ITCZ clusters one can combine the observed large-scale heat and moisture budgets of the cluster band region

with a cumulus ensemble parameterization model. Thus a considerable effort has been made to obtain representative estimates of these budgets since the late 1960's (WILLIAMS [15], REED and RECKER [13], NITTA [7], YANAI *et al.*, [16], NITTA and ESBENSEN [9], and NITTA [8]). One such an attempt was made during Phase 4 (13, 18–20, 22, and 28 July, 1969) of the Barbados Oceanographic and Meteorological Experiment (BOMEX).

The main purpose of this study is to demonstrate the variability of the A/B-scale mass, heat, and moisture budgets in two different A/B-scale situations within the ITCZ regime, obtained during BOMEX Phase 4. A compositing technique is used to distinguish a weakly disturbed class with weak or decaying cloud clusters from a strongly disturbed one characterized by mature clusters.

2. *Data*

BOMEX was conducted in May, June, and July 1969. This study uses the rawinsonde data and the surface observations of cloudiness for Phase 4 from 13 to 28 July. These data were provided by Dr. E. RASMUSSON, Mr. T. CARPENTER, and Mr. S. WILLIAMS at the Center for Experiment Design and Data Analysis (CEDDA) of the National Oceanic and Atmospheric Administration (NOAA).

In this study only the southernmost triangle of the Phase 4 fixed-ship array is considered, as shown in fig. 1. The rawinsonde data set consists of the soundings taken at each of the three ships — the Discoverer, the Mount Mitchell, and the Oceanographer. Measurements of temperature, humidity, and wind are available with a time interval of 3 hours for the following diurnal periods:

13 July 0300 GMT − 14 July 0000 GMT,
18 July 0300 GMT − 19 July 0000 GMT,
19 July 0300 GMT − 20 July 0000 GMT,
20 July 0300 GMT − 21 July 0000 GMT,
22 July 0600 GMT − 23 July 0300 GMT, and
27 July 1800 GMT − 28 July 1500 GMT.

The vertical range covered extends from the sea surface to 500 mb above it with a 10 mb resolution. If the original data values were more than three standard deviations from the mean at the same level, they were discarded. The missing and discarded data were interpolated linearly in the vertical, if possible. If not, the interpolation or extrapolation were performed in time. Approximately 20 per cent of the wind data has been interpolated or extrapolated. These data with a 20 mb vertical resolution were used to compute the A/B-scale mass, heat, and moisture budgets. The daytime rawinsonde humidity errors due to the radiative heating of
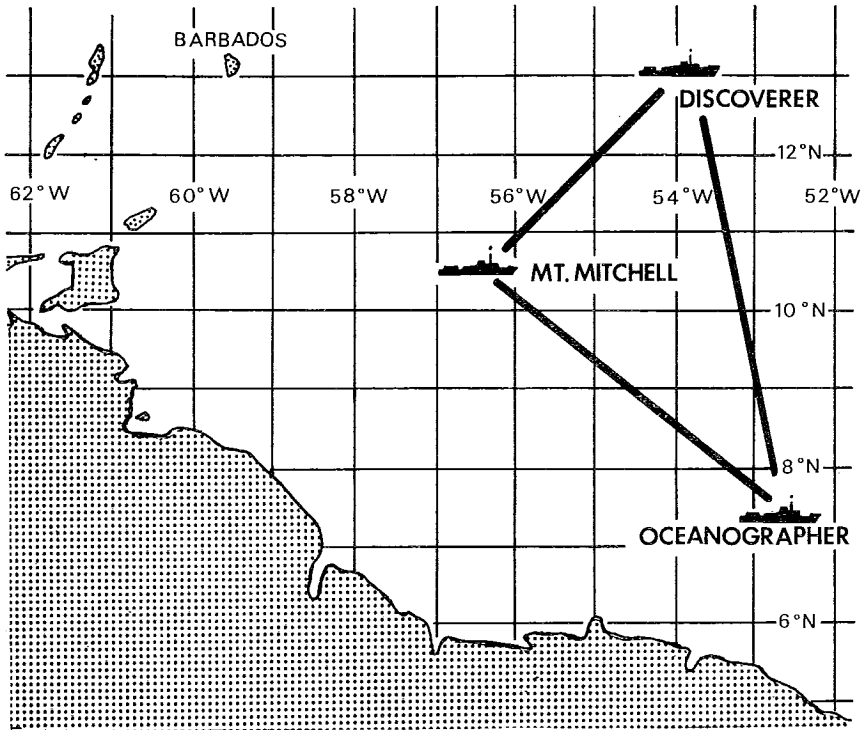
Fig. 1. The three southernmost ships of the fixed-ship array during BOMEX Phase 4
(NOAA/EDS, [11]).

the hygristor element (TEWELES [14]) were corrected during the final data
reduction process at CEDDA (NOAA/Environmental Data Service (EDS), [11]).
The corrected humidities are believed to be accurate within 5 per cent relative
humidity, but slightly biased during very cloudy conditions.

The radiation data set consists of a single average profile of the total radiative
heating as obtained by Dr. S. Cox.

3. Method of Analysis

For computations of the A/B-scale mass, heat, and moisture budgets methods
similar to those by YANAI et al. [16] and NITTA and ESBENSEN [9] are used.
The coordinate system is a p^*-system, where $p^* = p_s - p$ (p_s is the surface
pressure).

The area-averaged $p^\star$-velocity, $\overline{\omega^\star}$, is determined by using the mass continuity equation in the form

$$\overline{\nabla \cdot V} + \frac{\partial \overline{\omega^\star}}{\partial p^\star} = 0, \tag{1}$$

where over-bars denote area averages. However, the 500 mb cut-off prevents any meaningful corrections from $\overline{\omega^\star}$ being calculated. The area-averaged horizontal divergence and relative vorticity are computed from

$$\overline{\nabla \cdot V} = \frac{1}{A} \oint v_n \, dl \tag{2}$$

$$\bar{\zeta} = \frac{1}{A} \oint v_t \, dl, \tag{3}$$

where v_n and v_t are the normal and tangential wind components along the periphery of the triangle under consideration. The area of the triangle is A and the length of its periphery is denoted by $\oint dl$.

Defining the dry static energy s by

$$s \equiv c_p T + \phi \tag{4}$$

the equations of the dry static energy and moisture continuity averaged over the analyzed area are

$$\frac{\partial \bar{s}}{\partial t} + \overline{\nabla \cdot sV} + \frac{\partial \overline{s\omega^\star}}{\partial p^\star} - \frac{\overline{\partial p_s}}{\partial t} \frac{\partial \phi}{\partial p^\star} = Q_R + L(c - e) \tag{5}$$

$$\frac{\partial \bar{q}}{\partial t} + \overline{\nabla \cdot qV} + \frac{\partial \overline{q\omega^\star}}{\partial p^\star} = e - c, \tag{6}$$

where q is the mixing ratio, Q_R the heating due to radiation, c the rate of condensation per unit mass of air, e the rate of re-evaporation of cloud droplets, and L the latent heat of condensation.

The interaction between the A/B-scale fields and the cumulus convection is investigated by applying a residual technique to eqs. (5) and (6). These can be written in the form

$$Q_1 \equiv \frac{\partial \bar{s}}{\partial t} + \overline{\nabla \cdot sV} + \frac{\partial \bar{s}\,\overline{\omega^\star}}{\partial p^\star} - \frac{\overline{\partial p_s}}{\partial t} \frac{\partial \phi}{\partial p^\star} = Q_R + L(c - e) - \frac{\partial \overline{s'\omega^{\star\prime}}}{\partial p^\star} \tag{7}$$

$$Q_2 = -L\left[\frac{\partial \bar{q}}{\partial t} + \overline{\nabla \cdot q V} + \frac{\partial \bar{q}\,\overline{\omega^\star}}{\partial p^\star}\right] = L(c - e) + L\frac{\partial \overline{q'\omega^{\star\prime}}}{\partial p^\star}, \tag{8}$$

where primes denote deviations from the areal averages. In eqs. (7) and (8) it is
assumed that the horizontal subgrid-scale eddy transports of s and q can be
neglected. The terms $\overline{s'\omega^{*'}}$ and $\overline{q'\omega^{*'}}$ represent the vertical eddy transports of
heat and moisture both due to the cumulus convection in the cloud layer and the
turbulence in the subcloud layer. The apparent heating Q_1 and the apparent
moisture sink Q_2 can be evaluated from the large-scale rawinsonde data. Also Q_R
is known.

4. Classification of the A/B-scale fields

The analyzed area lay well within the ITCZ regime and was disturbed by cloud
clusters during the whole period under consideration. This is found from the day-
time (mainly near local noon), image enhanced, precision-display cloud photo-
graphs (not shown here) of ATS-3, produced at the University of Wisconsin, and
is also illustrated in the BOMEX Synoptic Weather Atlas (NOAA/EDS, [12]).

Fig. 2 shows the time-height distribution of the vertical velocity $\overline{\omega^*}$. Here no
time smoothing has been applied. For most days quite large temporal variations
of $\overline{\omega^*}$ can be seen. However, these variations cannot be compared satisfactorily
with the few cloud observations. From this general result July 13 and 20 emerge
as exceptions, the former predominantly with upward motions and the latter with
downdrafts. On these days the computed $\overline{\omega^*}$ profiles agree quite well with the
cloud observations.

Using the cloud observations and computed $\overline{\omega^*}$ profiles the available diurnal
periods are classified into two categories:

Class 1: The A/B-scale area is affected by weak or decaying cloud clusters.
  (20 July 0300 GMT – 21 July 0000 GMT and
  27 July 1800 GMT – 28 July 1500 GMT)

Class 2: The A/B-scale area is affected by a mature cloud cluster.
  (13 July 0300 GMT – 14 July 0000 GMT,
  18 July 0300 GMT – 19 July 0000 GMT,
  19 July 0300 GMT – 20 July 0000 GMT, and
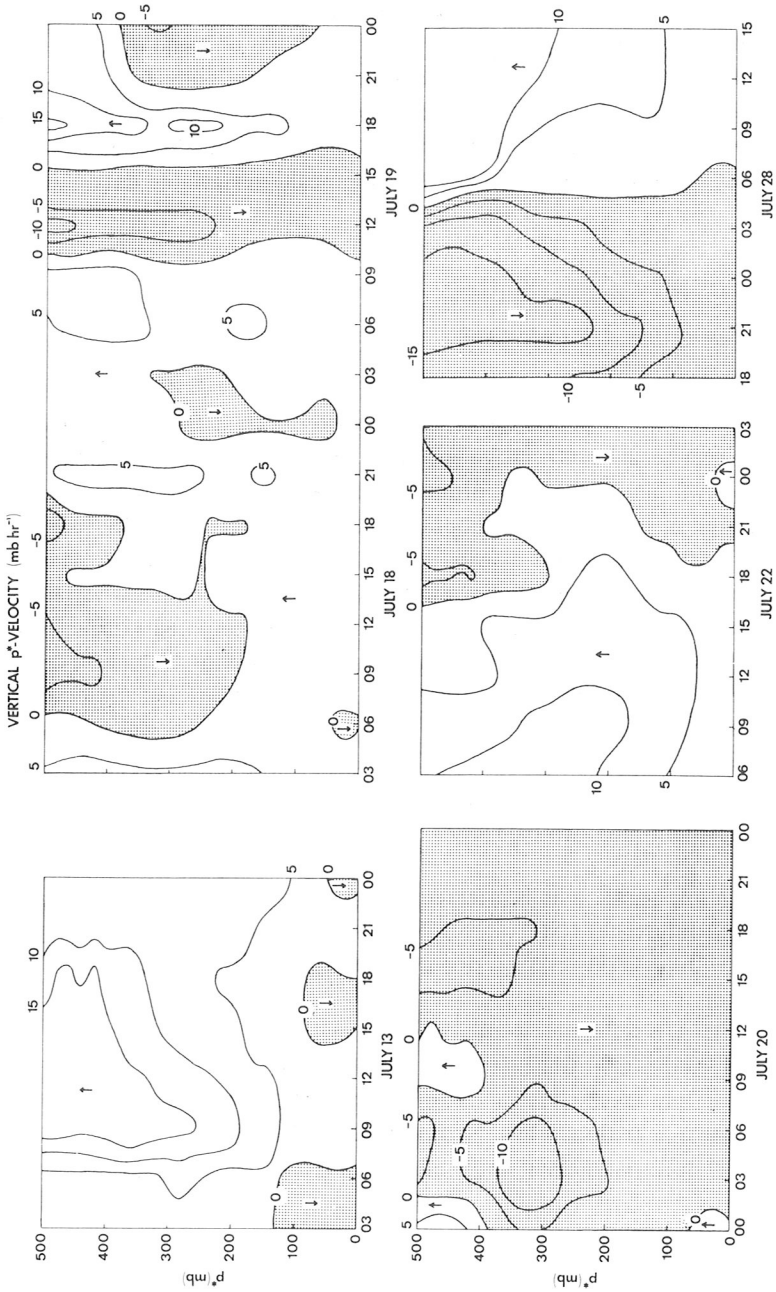 22 July 0600 GMT – 23 July 0300 GMT)

Fig. 2. Vertical time section of the area-averaged vertical p^*-velocity ($\overline{\omega^*}$). Shaded areas represent downward motions.

5. *The dry and moist static energy and the mean wind shear*

Defining the moist static energy h by

$$h \equiv c_p T + \phi + Lq \tag{9}$$

the mean profiles of the dry and moist static energy for the two classes are shown in figs 3a–b. This also includes the mean profiles of the saturation moist static energy $h^\star$ defined by

$$h^\star = c_p T + \phi + Lq^\star(p, T), \tag{10}$$

where $q^\star(p, T)$ is the saturation mixing ratio. According to NITTA and ESBENSEN [9] and MADDEN and ROBITAILLE [6] the vertical gradients of s and $h^\star$ can be used as measures of static stability for unsaturated and saturated air parcels, respectively.

For the weakly disturbed class 1 (sample size $N = 16$) the dry and moist static energy have almost constant values in a 40 mb thick layer closest to the sea surface. In particular the sharp decrease of $\tilde{h}$ ($\sim$ denotes time averaging) with height at $p^\star \approx 40$ mb indicates the top of the mixed layer. Thus the mixed layer of the weakly disturbed ITCZ is somewhat thinner than the mixed layer observed in the nearby trade-wind region of BOMEX Phase 3 during an undisturbed period (NITTA and ESBENSEN [9]). Above the mixed layer s increases with height. Between $p^\star = 180$ mb and $p^\star = 240$ mb $\tilde{h}$ decreases quite sharply with altitude, whereas $\tilde{h}^\star$ increases. Then a substantial decrease of moisture takes place within this stable layer. Higher up, between $p^\star = 300$ mb and $p^\star = 340$ mb, one finds a rapid increase of $\tilde{h}$ with height. Due to a decrease of $\tilde{h}^\star$ with altitude, the moisture increases here with height, a feature absent from the trade-wind region.

In the strongly disturbed class 2 ($N = 32$) the top of the mixed layer has weakened at $p^\star \approx 40$ mb so that in many soundings it is not at all detectable. Higher up, between $p^\star = 200$ mb and $p^\star = 280$ mb, the moisture decreases upwards. However, this decrease is weaker than the one for class 1. Consequently, the moisture content at $p^\star = 500$ mb is larger for class 2. The relatively large difference between $\tilde{s}$ and $\tilde{h}$ was also found by YANAI *et al.* [16] in the Marshall Islands.

It is well known that in addition to the static stability, the ambient wind shear has a considerable effect on the growth of convective clouds (COTTON [3]). Figs. 4a–b show the profiles of $\tilde{u}$ and $\tilde{v}$ for classes 1 and 2, respectively. According to the $\tilde{u}$ profiles the easterlies prevail at all levels both during weakly and strongly disturbed periods. The weak, easterly low-level jet characteristic of the nearby
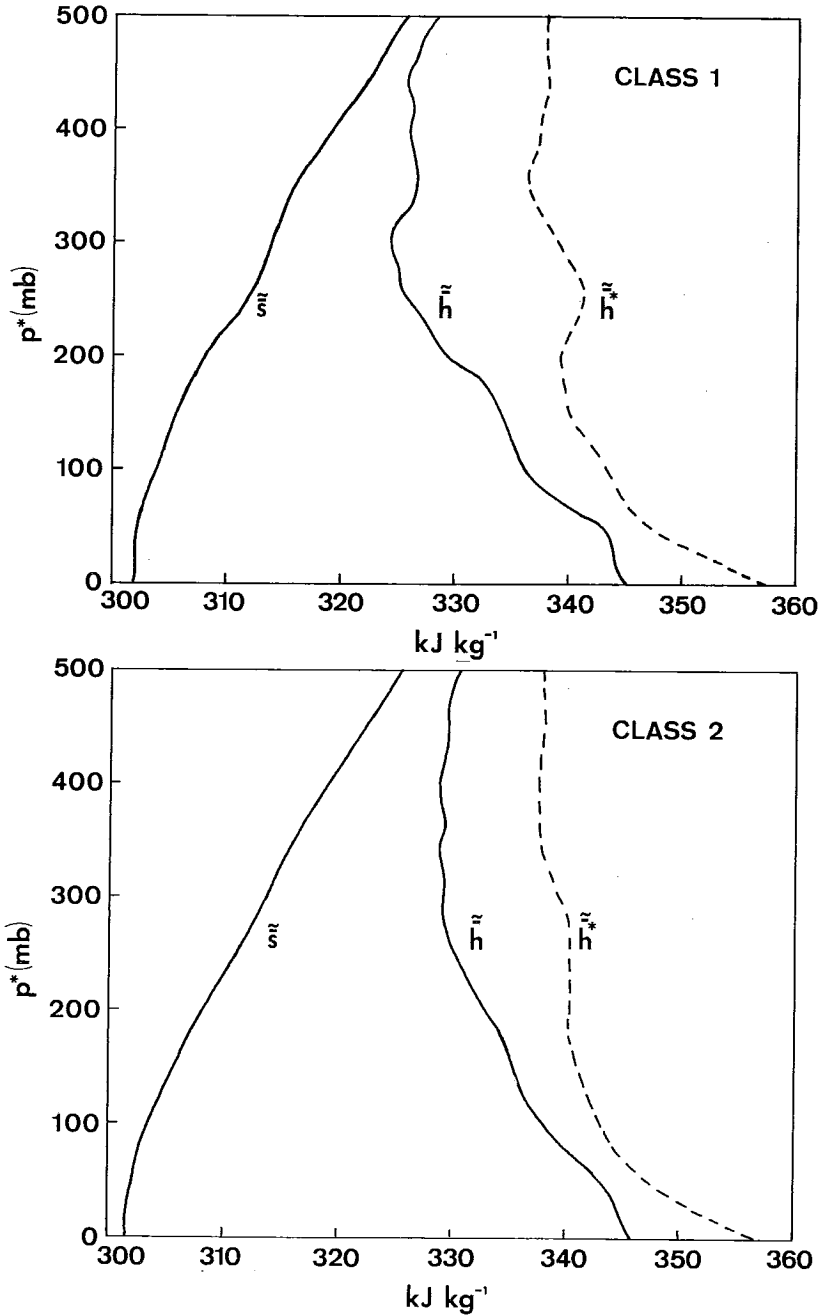
Fig. 3. Vertical mean profiles of dry static energy, moist static energy (both solid), and saturation moist static energy (dashed) ($\sim$ denotes time averaging).
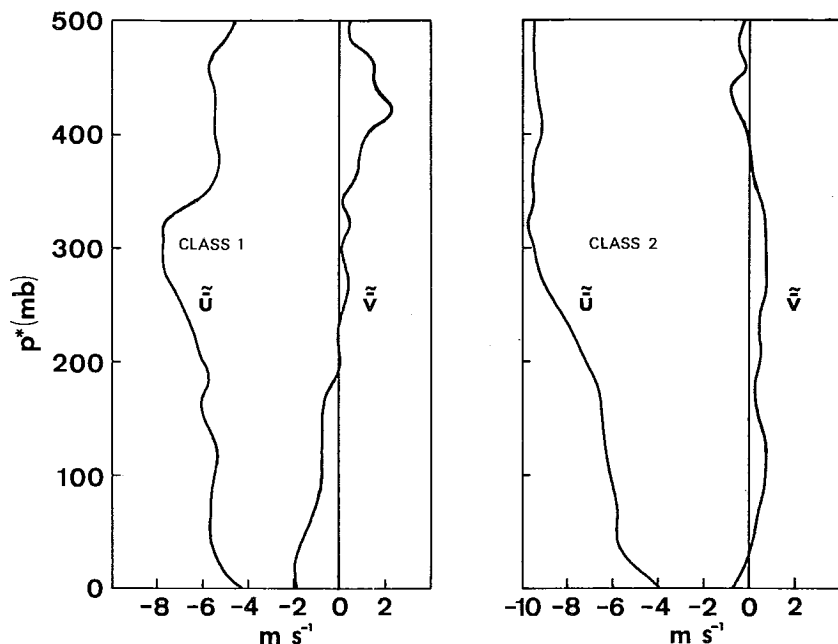   a) weakly disturbed class 1
    b) strongly disturbed class 2

Fig. 4. Vertical mean profiles of u and v.
a) weakly disturbed class 1
b) strongly disturbed class 2

trade-wind region during an undisturbed period of BOMEX Phase 3 (HOLLAND and RASMUSSON [4]) is pushed upwards for weak or decaying cloud clusters (class 1) in the ITCZ region of BOMEX Phase 4. However, this jet is considerably weaker than the one found by NITTA [8] for decaying cloud clusters (Period 2) in the GARP Atlantic Tropical Experiment (GATE) A/B-scale area. In class 2 an easterly shear extends from the surface up to $p^\star \approx 300$ mb. Above this shear layer $\tilde{u}$ is almost constant, and no strong easterly jet like the one for mature cloud clusters (Period 1) in the GATE A/B-scale area (NITTA [8]), is present in the lower troposphere.

The mean meridional wind and its shear are weak, as in the trade-wind region. During weakly disturbed periods (class 1) a northerly shear extends from the surface up to $p^\star = 420$ mb. On the other hand the $\tilde{v}$ profile shows a weak low-level northerly shear and a southerly shear above $p^\star = 300$ mb for class 2.

6. *Divergence, relative vorticity, and vertical velocity*

Fig. 5 illustrates the horizontal divergence profiles for the weakly and strongly disturbed classes 1 and 2, respectively. Table 1 also shows some values of $\overline{\widetilde{\nabla \cdot V}}$ with their standard deviations $s_{\overline{\widetilde{\nabla \cdot V}}}$. For class 1 divergence takes place below

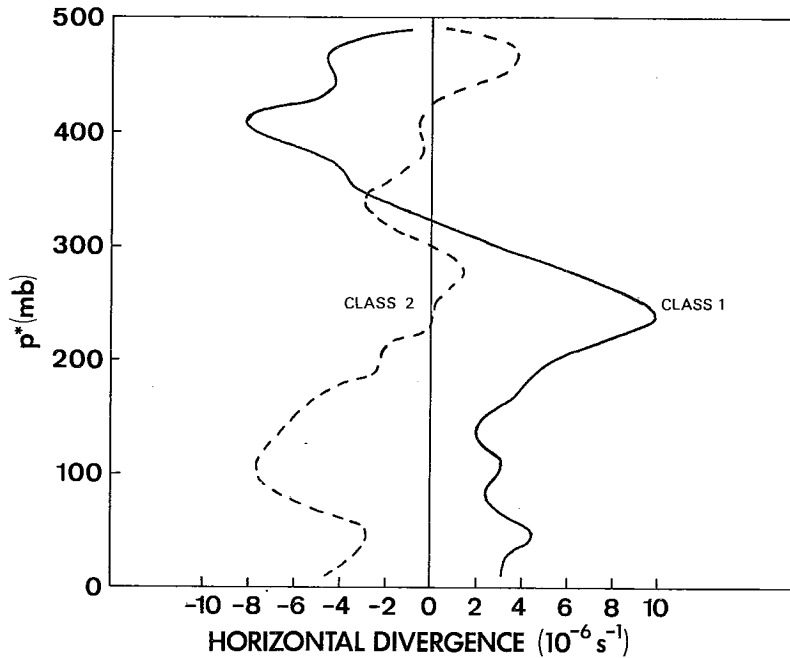Fig. 5. Vertical mean profiles of horizontal divergence for class 1 (solid) and class 2 (dashed).

Table 1. The mean values and their standard deviations for the horizontal difference of class 1 (N=16) and class 2 (N=32).

$p^\star$	Class 1		Class 2	
	$\overline{\widetilde{\nabla \cdot V}}$	$s_{\overline{\widetilde{\nabla \cdot V}}}$	$\overline{\widetilde{\nabla \cdot V}}$	$s_{\overline{\widetilde{\nabla \cdot V}}}$
mb	$10^{-6}s^{-1}$	$10^{-6}s^{-1}$	$10^{-6}s^{-1}$	$10^{-6}s^{-1}$
10	3.11	1.95	−4.61	1.47
90	2.57	2.36	−7.29	1.49
190	4.70	2.12	−2.52	1.63
290	4.35	2.62	1.01	1.94
390	−6.51	2.64	−0.42	2.18
490	−0.97	1.37	0.62	2.47

$p^\star = 320$ mb and convergence above it. Compared with the results obtained by NITTA [8], the profile resembles the one for decaying cloud clusters (Period 2). The largest difference is found in the layer below $p^\star = 100$ mb, where the profile of class 1 shows divergence instead of convergence. Taking into account the standard deviations of $\overline{\widetilde{\nabla \cdot V}}$ for class 1 the low-level divergence may well be too strong or actually weak convergence. On the other hand, one can say that there is a divergent layer between $p^\star = 200$ mb and $p^\star = 280$ mb and a convergent layer extending from $p^\star = 380$ mb to $p^\star = 420$ mb. For class 2 convergence takes place from the surface up to $p^\star \approx 200$ mb and has its highest values above the surface, between $p^\star = 80$ mb and $p^\star = 150$ mb. Further up the divergence values are relatively small. A comparison with the profile of the disturbed period in the nearby trade-wind region during BOMEX Phase 3 (NITTA and ESBENSEN [9]) reveals that the convergence layer closest to the surface becomes thicker towards the ITCZ. For mature cloud clusters (Period 1) in the GATE A/B-scale area (NITTA [8]) the results indicate a 250 mb thick layer of convergence. This thickness agrees fairly well with the result obtained for class 2. However, in the GATE A/B-scale area the level of the strongest convergence is at the surface, whereas in the southernmost triangle of BOMEX Phase 4 as well as in the Marshall Islands (YANAI et al., [16]) this level is found slightly above the surface.

Fig. 6 shows the vertical distribution of the relative vorticity $\widetilde{\zeta}$. Both for class 1 and class 2 the relative vorticity is positive almost throughout the layer, especially below $p^\star \approx 300$ mb. Furthermore $\widetilde{\zeta}$ has considerably higher values for class 2 than class 1 below $p^\star = 40$ mb. In the Marshall Islands the result by YANAI et al. [16] shows the positive relative vorticity decreases with height below $p^\star \approx 300$ mb. This agrees fairly well with the result of class 1. On the other hand NITTA [8] obtains larger positive $\widetilde{\zeta}$ values for all periods in the GATE A/B-scale area.

The vertical velocity $\omega^\star$ results are illustrated in fig. 7. In class 1 downward motion predominates throughout the layer, whereas upward motion extends from the surface to the top of the layer in class 2. Owing to the large standard deviations of $\overline{\nabla \cdot V}$ values for class 1, the predominant downward motion for the whole layer is probably partly spurious, especially close to the surface. For the decaying cloud clusters (Period 2) in the GATE A/B-scale area NITTA [8] finds upward motion extending from the surface up to $p^\star \approx 280$ mb with downward motion above it beyond $p^\star = 500$ mb. The vertical velocity profile by YANAI et al. [16] agrees with the result of class 2. NITTA [8] also obtains upward motion throughout the troposphere for mature cloud clusters (Period 1). A comparison with the nearby trade-wind region of BOMEX Phase 3 (NITTA and ESBENSEN [9]) during a disturbed period reveals that the upward motion becomes vertically far more predominant as one approaches the ITCZ.
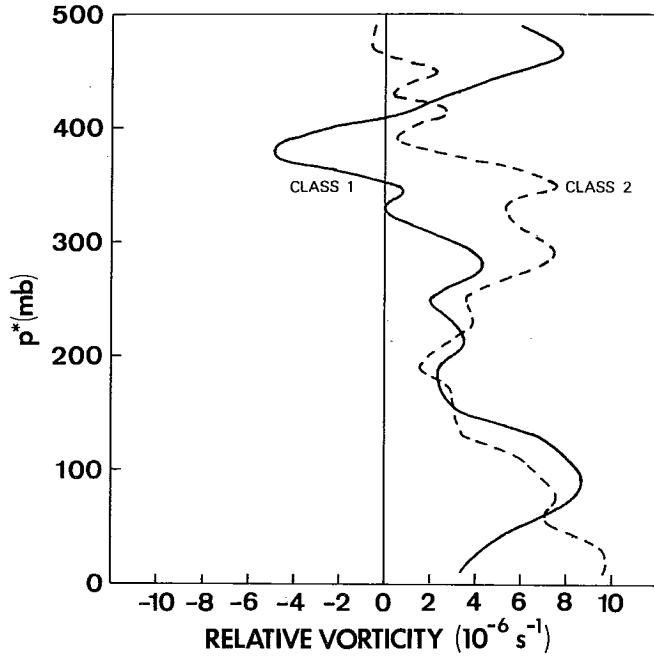
Jaakko Helminen

Fig. 6. Vertical mean profiles of relative vorticity for class 1 (solid) and class 2 (dashed).
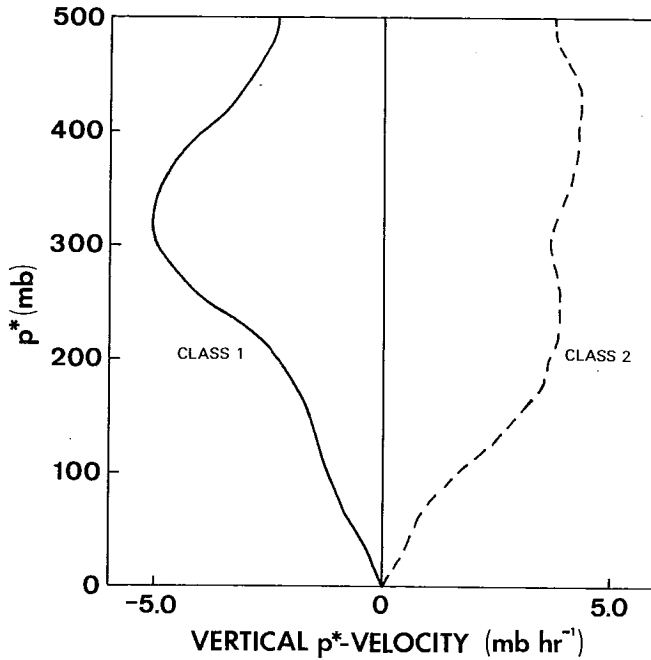

Fig. 7. Vertical mean profiles of vertical $p^\star$-velocity for class 1 (solid) and class 2 (dashed).
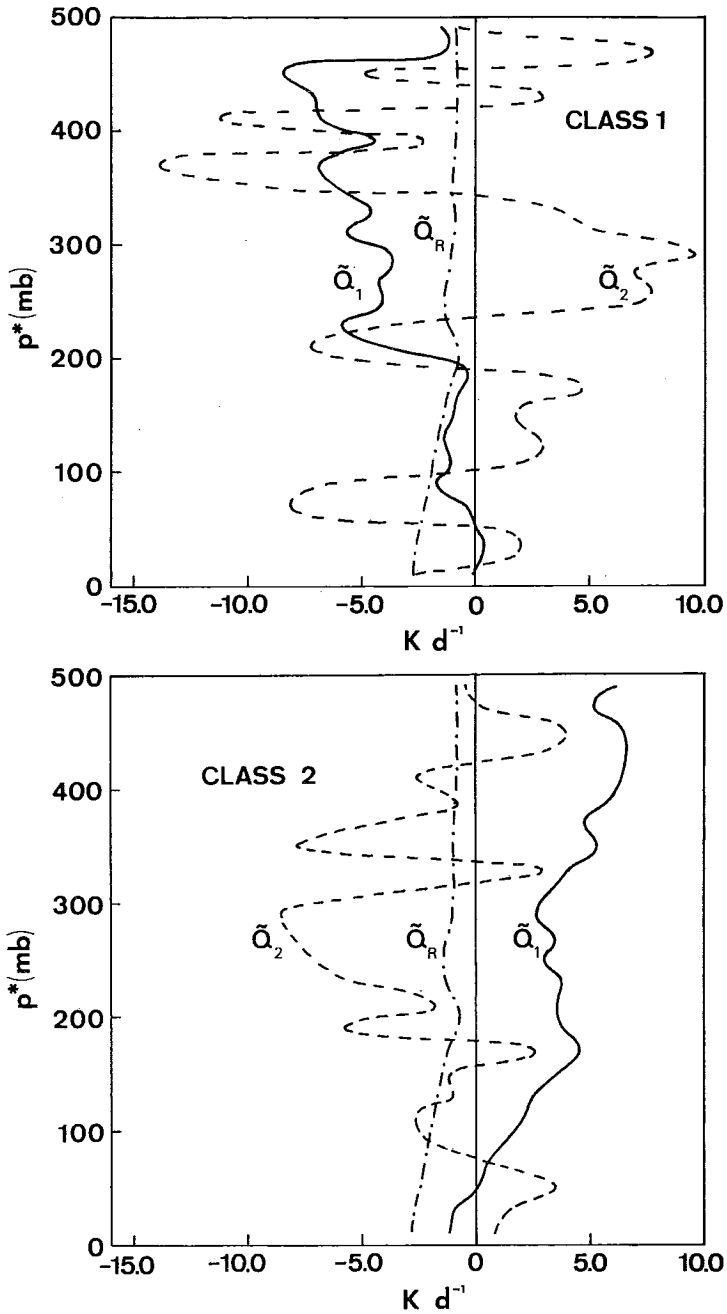
Fig. 8. Vertical mean profiles of apparent heat source (solid), apparent moisture sink
(dashed), and radiational heating (dash-dotted).
    a) weakly disturbed class 1, b) strongly disturbed class 2

7. *Heat and moisture budgets*

The apparent heat source $\widetilde{Q}_1$ and the apparent moisture sink $\widetilde{Q}_2$ profiles for the two classes are shown in figs. 8a—b. The radiative heating $\widetilde{Q}_R$ is also drawn in these diagrams. For both classes the values of $\widetilde{Q}_2$ appear widely scattered in the vertical direction. Also the standard deviations of $\widetilde{Q}_2$ are large. A closer look at the separate terms of $\widetilde{Q}_2$ reveals the predominance of the horizontal and vertical flux terms at individual levels. Unfortunately these moisture fluxes and their partial cancellation cannot be assessed with sufficient accuracy in the southernmost triangle of BOMEX Phase 4.

The profiles of $\widetilde{Q}_1$ are smoother than those of $\widetilde{Q}_2$. For class 1 there is a large apparent heat sink between $p^\star = 200$ mb and $p^\star = 480$ mb. This cooling is probably caused by the re-evaporation of cloud droplets which detrain from the decaying cloud clusters. Unfortunately this cannot be verified by the $\widetilde{Q}_2$ profile, which is partly spurious. However, despite the differences in thickness and height, the cooling layer agrees fairly well with the one obtained by NITTA [8] for decaying cloud clusters (Period 2) in the GATE A/B-scale area. The average cooling rate due to $\widetilde{Q}_1$ for the 500 mb thick layer is about -3.5 K per day and the average precipitation $\widetilde{\widetilde{P}} = 4.2$ mm d^{-1}. In class 2 a large apparent heat source extends from $p^\star = 50$ mb upwards, and $\widetilde{Q}_1 - \widetilde{Q}_R$ is positive in the whole layer under consideration. This apparent heat source may be caused by the adiabatic warming due to compensating downward motion in the environment of the cumulus clouds. The $\widetilde{Q}_1$ profile of YANAI *et al.* [16] for the Marshall Islands as well as the one by NITTA [8] for mature cloud clusters (Period 1) in the GATE A/B-scale area have a shape similar to the one obtained for class 2. The average heating rate due to $\widetilde{Q}_1$ for the layer considered is approximately 3.0 K per day, which agrees well with the value obtained by YANAI *et al.* [16]. On the other hand the value is considerably less than the one obtained by NITTA [8] for mature cloud clusters. The average precipitation for class 2 is $\widetilde{\widetilde{P}} = 0.7$ mm d^{-1}.

8. *Conclusions and remarks*

In this work the A/B-scale mass, heat, and moisture budgets have been calculated for the southernmost triangle of the BOMEX Phase 4 in an area which represents the ITCZ region. In the 500 mb thick column under consideration the mean results show a large variability. For class 1 with weak or decaying cloud clusters, a low-level easterly jet at $p^\star = 300$ mb and a 40 mb thick mixed layer can be detected. However, the predominant, fairly strong divergence and downward motion are partly spurious. The heat budget profile $\widetilde{Q}_1$ ($\sim$ denotes time averaging) shows a

large apparent heat sink between $p^\star = 200$ mb and $p^\star = 480$ mb. This cooling is probably partly caused by decaying cloud clusters. In class 2, which is characterized by mature cloud clusters, no low-level zonal jet or mixed layer were found. Strong low-level convergence, large positive relative vorticity, and upward motion also exist. The heat budget profile $\tilde{Q}_1$ and the profile of the total radiative heating $\tilde{Q}_R$ give a positive $\tilde{Q}_1 - \tilde{Q}_R$ for the whole layer. This may be caused by the adiabatic warming due to compensating downward motion in the environment of the cumulus clouds. For the most part, the moisture budget results show systematic errors and a large variability. Further attempts to calculate the vertical total eddy heat flux due to subgrid-scale eddies lead to meaningless profiles and are not shown. Instead some causes of the failure are discussed.

The satellite cloud photographs reveal that one characteristic feature of the ITCZ regime is the large areal and temporal variability of the events. To resolve the various stages of these events careful scientific planning of experiments is needed, like the one implemented in the GATE (see *e.g.* NITTA [8]). Compared with the GATE A/B-scale network the southernmost large triangle of BOMEX Phase 4 is too coarse to assess the divergence and the fluxes in the ITCZ region. This is an important reason for the large standard deviations and systematic errors in the results. Also the variations in humidity at the corners of the triangle may not be areally representative for the large triangle and cause further variability and errors in the moisture fluxes.

To classify the temporal variations it is essential to have satellite cloud photographs simultaneous with the soundings. During BOMEX Phase 4 only irregular daytime cloud photographs were available. This and the possible large diurnal variations of the large-scale variables (for BOMEX Phase 3 see NITTA and ESBENSEN [10]) restricted the classification possibilities to 24-hour periods, which increased the standard deviations of the mean values. Also, some systematic errors are unavoidable with such a rough classification, based mainly on the activity of the cloud clusters.

REFERENCES

1. ARAKAWA, A. and W.H. SCHUBERT, 1974: Interaction of a Cumulus Cloud Ensemble with the Large-Scale Environment, Part I. *J. Atmos. Sci.,* 31, 647–701.

2. BETTS, A.K., 1973: Non-precipitating cumulus convection and its parameterization. *Quart. J. Roy. Meteor. Soc.,* 99, 178–196.

3. COTTON, W.R., 1975: Theoretical Cumulus Dynamics. *Rev. Geophys. Space Phys.,* 13, 419–448.

4. HOLLAND, J.Z. and E.M. RASMUSSON, 1973: Measurements of the atmospheric mass, energy, and momentum budgets over a 500-km square of tropical ocean. *Mon. Wea. Rev.,* 101, 44–55.

5. JOINT ORGANIZING COMMITTEE STUDY GROUP, 1970: The Planning of GARP Tropical Experiments. Appendix I. *GARP Publications Series No. 4,* 33–39, ICSU/WMO.

6. MADDEN, R.A. and F.E. ROBITAILLE, 1970: A Comparison of the Equivalent Potential Temperature and the Static Energy. *J. Atmos. Sci.,* 27, 327–329.

7. NITTA, T., 1972: Energy budget of wave disturbances over the Marshall Islands during the years of 1956 and 1958. *J. Meteor. Soc. Japan,* 50, 71–84.

8. – » –, 1977: Response of Cumulus Updraft and Downdraft to GATE A/B-Scale Motion Systems. *J. Atmos. Sci.,* 34, 1163–1186.

9. – » –and S. ESBENSEN, 1974a: Heat and Moisture Budget Analyses Using BOMEX Data. *Mon. Wea. Rev.,* 102, 17–28.

10. – » –, 1974b: Diurnal Variations in the Western Atlantic Trades during the BOMEX. *J. Meteor. Soc. Japan,* 52, 254–257.

11. NATIONAL OCEANIC AND ATMOSPHERIC ADMINISTRATION/ENVIRONMENTAL DATA SERVICE, 1975a: BOMEX Permanent Archive: Description of Data. *NOAA Technical Report* EDS 12. NOAA/EDS.

12. – » –, 1975b: *BOMEX Synoptic Weather Atlas.* NOAA/EDS.

13. REED, R.J. and E.E. RECKER, 1971: Structure and properties of synoptic-scale wave disturbances in the equatorial western Pacific. *J. Atmos. Sci.,* 28, 1117–1133.

14. TEWELES, S., 1970: A spurious diurnal variation in radiosonde humidity records. *Bull. Amer. Meteor. Soc.,* 9, 836–840.

15. WILLIAMS, K.T., 1970: A statistical analysis of satellite-observed trade wind cloud clusters in the western north Pacific. *Atmos. Sci. Paper No. 161, Colorado State University,* Fort Collins, 80 pp.

16. YANAI, M., ESBENSEN, S. and J.-H. CHU, 1973: Determination of bulk properties of tropical cloud clusters from large-scale heat and moisture budgets. *J. Atmos. Sci.,* 30, 611–627.